Magnitude Modulation for VSAT's Low Back-Off Transmission

Marco Gomes, Francisco Cercas, Vitor Silva, and Martin Tomlinson

Abstract: **This paper addresses the problem of controlling the envelope's power peak of single carrier modulated signals, band limited by root-raised cosine (RRC) pulse shaping filters, in order to reduce power amplifier back-off for very small aperture terminals ground stations. Magnitude modulation (MM) is presented as a very efficient solution to the peak-to-average power ratio problem. This paper gives a detailed description of the MM concept and its recent evolutions. It starts by extending the look-up-table (LUT) based approach of the MM concept to M-ary constellations with $M \leq 16$. The constellation and RRC symmetries are explored, allowing considerable reduction on LUT computation complexity and storage requirements. An effective multistage polyphase (MPMM) approach for the MM concept is then proposed. As opposed to traditional LUT-MM solutions, MM coefficients are computed in real-time by a low complexity multirate filter system. The back-off from high-power amplifier saturation is almost eliminated (reduction is greater than 95%) with just a 2-stage MPMM system even for very demanding roll-off cases (e.g., $\alpha = 0.1$). Also, the MPMM is independent of modulation in use, allowing its easy application to constellations with $M > 16$.**

Index Terms: **Back-off, magnitude modulation (MM), multirate filtering, peak-to-average power ratio (PAPR), very small aperture terminals (VSAT).**

I. INTRODUCTION

Peak power reduction and spectral efficiency are two of the major issues in practical communications system design. A high peak-to-average power ratio (PAPR) puts stringent requirements on the transmitter's digital-to-analog converter (DAC) and high-power amplifier (HPA), increasing these system's components cost, whilst terribly degrades system's power efficiency. This problem is actually emphasized when, in order to meet the currently growing demands for higher data rates (and so higher spectral efficiency), very low roll-off root-raised cosine (RRC) pulse shaping filters and high-order constellations are used, since these lead to an increase on the signal's PAPR.

We focus our study on the problem of achieving low PAPR with strictly band-limited single-carrier (SC) signals, often selected as the preferred solution for communications where transmitter's power consumption might be a concern, such as very small aperture terminals (VSAT) and small mobile devices. Data magnitude modulation (MM) prior to RRC filtering is one of the techniques used to decrease PAPR in SC transmissions. The MM concept was proposed in the end nineties by Miller *et al.* [1], [2], who, based on it, developed an adaptive peak-suppression algorithm that works well for phase shift keying (PSK) and generalized PSK constellations. An efficient look-up-table (LUT) implementation of the MM technique was later proposed by Tomlinson *et al.* [3], [4] and applied with success to quadrature phase shift keying (QPSK) and offset QPSK (OQPSK) constellations.

This paper presents an improved evolution of the MM technique that can be easily included in currently operating and future VSAT terminals. We start by showing that it is possible to meliorate the LUT-MM method and apply it to higher-order non-constant amplitude constellations, even considering the huge number of symbol combinations. Resulting from RRC being driven by a sequence of data symbols varying not only in phase but also in magnitude, the control of envelope's peak-power at RRC output is more complex. In order to cope with the additional complexity, new clipping limits were proposed [5] and the method's capability to avoid phase modulation was improved [6]. In addition, we also show that a considerable reduction on LUT's computation complexity and storage requirements can be achieved by exploring the constellation's symmetry and the RRC's linear phase characteristic. A performance evaluation, focusing PAPR, back-off and bit error rate (BER), of the improved LUT-MM technique applied to 16-quadrature amplitude modulation (QAM) and 16-amplitude and phase shift keying (APSK) constellations, validates the adopted approach.

The recent highly efficient multirate LUT-less MM scheme will be then described [7], [8]. That method, designated by multistage polyphase MM (MPMM), computes the MM coefficients in real time. A simple polyphase filter system predicts undesirable peak excursions at the output of the RRC filter and adjusts accordingly the amplitude of the symbols at the RRC input. Experimental results, here presented, show that, by using only two MPMM base-system blocks, it is possible to eliminate almost completely the need to use back-off from the HPA saturation point, even at very low roll-off values. In addition, it became clear that the MPMM scheme is independent from the modulation used, since the polyphase filter structure only depends on the RRC impulse response, and so it overcomes the limitations of the traditional LUT-MM technique.

This paper is organized as follows: Section II presents a detailed overview of the MM concept and describe the basic building blocks of an MM system. LUT-MM technique is discussed in Section III. Several improvements made up to

Manuscript received April 30, 2010.

M. Gomes wishes to acknowledge Fundação para a Ciência e a Tecnologia (FCT), for partially supporting this work under Ph.D. Grant SFRH/BD/38338/2007.

M. Gomes and V. Silva are with Instituto de Telecomunicações at the Department of Electrical and Computer Engineering, University of Coimbra, 3030-290 Coimbra, Portugal, email: {marco, vitor}@co.it.pt.

F. Cercas is with the ISCTE-IUL and Instituto de Telecomunicações, 1649-026 Lisbon, Portugal, email: francisco.cercas@lx.it.pt.

M. Tomlinson is with the Department of Communications and Electronic Engineering, University of Plymouth, Plymouth PL4 8AA, U.K., email: M.Tomlinson@plymouth.ac.uk.

1229-2370/10/$10.00

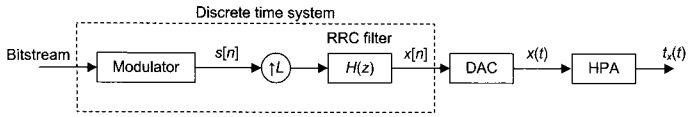

Fig. 1. Generic transmitter's system block diagram.

Table 1. PAPR contributions.

Constellation contribution					
Constellation	M-PSK	16-APSK[1]	16-QAM	32-APSK[2]	32-QAM
$\text{PAPR}_{\text{Const}}$	0 dB	1.1 dB	2.6 dB	2.1 dB	2.3 dB
RRC contribution					
RRC roll-off	0.1	0.2	0.3	0.4	0.5
PAPR_{RRC}	7.5 dB	5.8 dB	4.6 dB	3.7 dB	3.4 dB

LUT-MM to handle higher order constellations are explained. Section IV presents the recently proposed high performance MPMM method and its main features are addressed. Experimental MM results are included in both sections. Finally, main conclusions are summarized.

II. THE MAGNITUDE MODULATION PRINCIPLE

The underlying principles of data magnitude modulation applied to SC communications are presented in this section. The generic block diagram of a typical SC transmitter is shown in Fig. 1. In SC systems, the main contribution to PAPR results from RRC bandwidth limitation that gives rise to undesirable envelope variations in transmitted signal $x[n]$ that drives the transmitter's DAC+HPA block.

The PAPR of the transmitted signal $x[n]$, prior to DAC, is defined as

$$\text{PAPR} = 10\log_{10}\left[\frac{\max|x[n]|^2}{E\left(|x[n]|^2\right)}\right] \text{ (dB)} \tag{1}$$

and it is the sum of two components: $\text{PAPR}_{\text{Const}}$ and PAPR_{RRC}, due to the constellation and the RRC filter, respectively, which are evaluated as

$$\text{PAPR}_{\text{Const}} = 10\log_{10}\left[\frac{\max\limits_{i=1,\cdots,M}|S_i|^2}{\frac{1}{M}\sum\limits_{i=1}^{M}|S_i|^2}\right] \text{ (dB)}, \tag{2}$$

$$\text{PAPR}_{\text{RRC}} = 10\log_{10}\left[\frac{\max\limits_{i=0,\cdots,L-1}\left(\sum\limits_{n=0}^{2N}|h[nL+i]|\right)^2}{\frac{1}{L}\sum\limits_{n=0}^{2NL}|h[n]|^2}\right] \tag{3}$$

where S_i, with $i = 1, \cdots, M$ are the symbols of a M-ary constellation, $h[n]$ is the impulse response of the pulse shaping RRC filter and $L \in \mathbb{N}$ is the oversampling rate. It is also assumed, without loss of generalization, a type I linear phase finite impulse response (FIR) RRC filter [9] with $2NL + 1$ coefficients, i.e., $h[n]$ spreads over $2N + 1$ symbols.

Both contributions are shown in Table 1. It is clear from (3) that $\text{PAPR}_{\text{Const}}$ is null for constant amplitude constellations, such as M-PSK. However, for higher order modulations, it contributes with a non-negligible value to the total PAPR value, as shown in Table 1. Nevertheless, the major contribution to PAPR comes from RRC pulse shaping, especially when considering roll-off (α) values in the range of interest, $\alpha \leq 0.3$. In practice, the HPA should be able, at least, to handle $\text{PAPR}_{\text{Const}}$, i.e., if the multirate pulse shaping system (L up-sampler followed by filter $h[n]$) has unitary power gain, $G_{\text{RRC}} = 1$, then maximum amplitude symbols (with amplitude denoted as $A_{\max}$) at the output of modulator (Fig. 1) should suffer no distortion, if they are directly fed at the HPA input. The main goal of any PAPR reduction technique for SC transmission is, therefore, to cancel this undesirable PAPR_{RRC} contribution, eliminating the need to back-off from HPA saturation, which can be expressed as

$$\textit{Back-off} = 10\log_{10}\left[\frac{\max|x[n]|^2}{(A_{\max}^2 G_{\text{RRC}})}\right] \text{ (dB)}. \tag{4}$$

A. PAPR Reduction Approaches

Different strategies can be followed in order to control the envelope excursion of transmitted signal $x[n]$ and hence decrease signal's PAPR. Since the main contribution to PAPR results from Nyquist pulse shaping bandwidth limitation, some of the proposed solutions try to decrease the PAPR by optimizing these filters [11], [12]. The remaining strategies can be categorized in two main groups: Post-filtering and pre-filtering processing techniques.

The use of post-filtering peak power reduction techniques may give rise to spectral spreading causing loss of bandwidth efficiency and undesirable adjacent channel interference. On the contrary, by making signal adjustments prior to filtering, we do not affect bandwidth of signal $x[n]$ guaranteeing operation within government allocated limits. However, these adjustments must take into account RRC impulse response $h[n]$ in order to prevent peak regrowth that may be caused by this filtering stage.

Regarding the latter strategy, two different approaches are usually followed: Trellis coding (TC) [13], [14] and MM [1]–[4]. TC techniques try to avoid critical sequences of modulated symbols that cause peak envelope excursions at the RRC's output. However, such solutions are complex, with a high computational overhead and difficult to include on currently operating radio transmission systems. In addition, they require constellation's redundancy, with some bits being used for shaping control, which implies a reduction on the transmitted information rate. As an example, the 8-PSK trellis coding technique proposed in [14] requires the use of 1 bit per transmitted symbol, only for shaping control, in order to achieve the best performance. The maximum information rate of 8-PSK signaling is thus in fact reduced by $2/3$, corresponding in practice to the information rate of a 4-ary constellation.

When compared to state-of-the-art trellis PAPR reduction techniques, MM shows similar PAPR reduction gains, however, with major advantages [15]. MM operates on modulator's output symbols providing adjusted symbols to the RRC block, i.e., it is a simple processing block fitted between the modulator and the RRC filter. Therefore, it can be easily included in currently

[1] 16-APSK digital video broadcasting-satellite-second generation (DVB-S2) constellation with $\gamma = 3.15$ [10].

[2] 32-APSK DVB-S2 constellation with $\gamma_1 = 2.84$ and $\gamma_2 = 5.27$ [10].

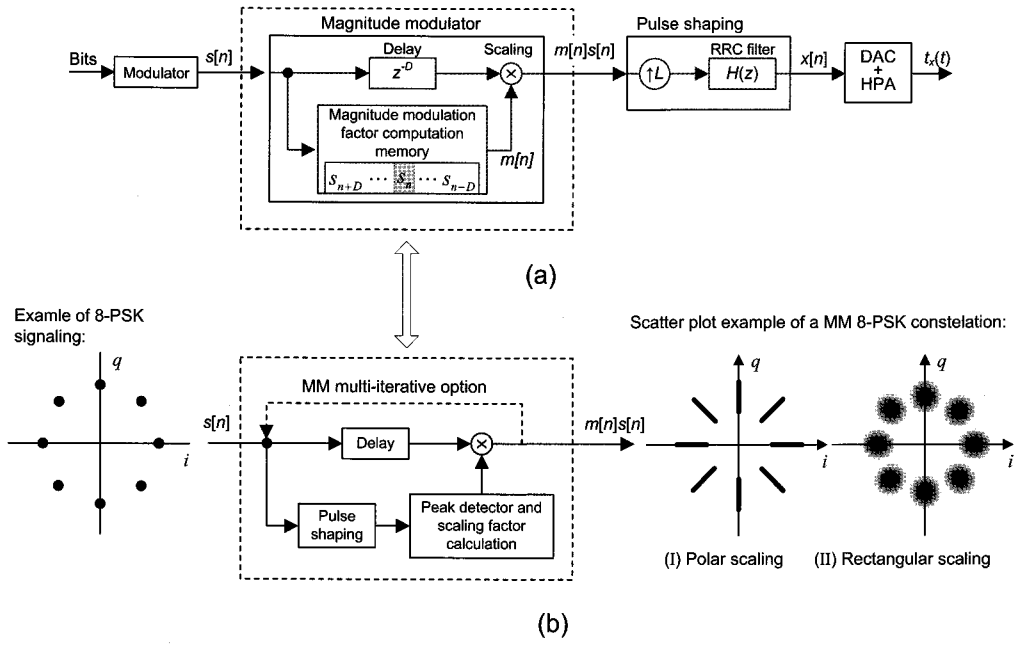

Fig. 2. (a) Generic transmitter's system block diagram including MM and (b) underlying principles of MM processing.

operating transmitter systems, without the need to replace the equipment already installed, which constitutes a very important advantage, from both system and economical points of view. In addition, it is possible to take advantage of the systems' existing forward error correction (FEC) capabilities in order to efficiently compensate the increase sensitivity to noise resulting from MM. Hence, no further FEC is needed, which means that MM doesn't imply a penalty reduction on the information rate.

B. Magnitude Modulation

Fig. 2 illustrates the functional diagram and the basic building blocks of a typical digital communication transmitter system using the MM concept [1]–[4]. The MM block adjusts the amplitude of the in-phase (I) and quadrature (Q) components of each modulator's output symbol

$$s[n] = s^I[n] + js^Q[n] \tag{5}$$

so as to suppress peaks in the RRC's output signal $x[n] \in \mathbb{C}$ to be transmitted.

The computation of the best MM coefficient $m[n]$ to apply to each symbol $s[n]$, can be accomplished by carrying out a procedure similar to the one proposed by Miller *et al.* [1], [2], that is presented in Fig. 2(b). The method is composed of three steps

1. Pulse shaping;
2. Peak detection and scaling factor calculation;
3. Scaling.

B.1 Pulse Shaping

As referred, by performing PAPR control by signal adjustment prior to filtering, in order to prevent peak regrowth at RRC's output, the response of the pulse shaping filter to the sequence $s[n]$ must be predicted. Hence, all samples (starting by the one to be magnitude modulated) that combine with the pulse shape to produce significant signal magnitude within the symbol interval of interest must, therefore, be considered in the computation of the MM coefficient. That's the reason why Fig. 2(a) shows a generic scheme of a MM system that looks at D past and future symbol neighbors[1] of s_n when computing MM coefficient m_n to apply to s_n. Hence, in this case, a delay of DT_{SYMB} is introduced by the MM technique, with T_{SYMB} denoting the symbol duration time.

The MM's processing delay D is usually small since it depends mainly on the time duration in which the RRC impulse response maintains significant non-zero amplitude values. However, if the MM procedure is made iterative as shown in Fig. 2(b), it increases k times, with k being number of iterations performed per MM factor computation.

B.2 Peak Detection and Scaling Factor Calculation

Computation of the MM coefficients is made on a T_{SYMB}-interval basis. However, according to the Nyquist theory, pulse shaping has to be performed at a higher sampling rate $1/T_{\text{SMPL}} = L/T_{\text{SYMB}}$, with $L \geq 2$ being the up-sampler factor of the rate expansion prior to RRC filtering. The RRC output symbol interval of interest, i.e., the one during which the contribution of symbol s_n (that is to be MM) is more notorious, it is therefore composed of L samples. This set of samples, and possibly also the ones from the neighboring intervals in its close vicinity (where influence of s_n can still be strongly felt), are analyzed in order to detect any peak excursion exceeding a specified threshold A.

Two different types of analysis may be performed: Polar and rectangular. Polar analysis compares the amplitude of the complex RRC's output samples with the specified threshold A (polar threshold), while rectangular analysis monitors independently the amplitude of the I and Q components of those samples, com-

[1]Hereafter, whenever there is doubt about we may be referring to a discrete time sequence $s[n]$ or to the particular sample of that sequence at instant n, we will denote the sample as s_n.

paring them against the rectangular thresholds, A_I and A_Q, respectively. Rectangular thresholds are usually chosen in order to guarantee that the final MM signal, $x[n]$, has an amplitude lower than the polar threshold A. However, polar analysis provides a fine control of signal magnitude.

If the threshold is exceeded, the algorithm calculates the symbol scale factor m_n to apply to s_n. A simple procedure consists on scaling down s_n by a factor

$$m_n = \frac{A}{A_s} \tag{6}$$

where A_s is the amplitude of the maximum peak detected during the analysis' interval. This value is named as MM factor or MM coefficient.

A better MM factor m_n may be obtained by employing more complex algorithms, such as the one proposed by Miller *et al.* [1], [2] and the recent MPMM [7], [8] that we present in Section IV. For example, Miller's algorithm considers the maximum signal excursion occurring to the left and to the right of symbol s_n during the analysis' interval, and computes m_n based on the amplitude of those two peaks and their relative time distance to the symbol s_n.

B.3 Scaling

Scaling of the data symbols can also follow two different strategies, with symbols being scaled solely in the magnitude (polar scaling) or both magnitude and phase (rectangular scaling).

Polar scaling multiplies both the I and Q components of symbol s_n by the same factor $m_n \in \mathbb{R}$ in order to avoid phase modulation. The equivalent complex digital baseband MM signal, after filtering, and prior to digital-to-analog (D/A) conversion, is therefore given by

$$x[n] = \left[\sum_k m[k]\, s[k]\, \delta[n - kL]\right] * h[n]\,. \tag{7}$$

Alternatively, the amplitude of the I and Q components may be altered independently resulting in changes to both the magnitude and the phase of s_n. The equivalent complex digital baseband MM signal using rectangular scaling can be expressed as

$$x[n] = \left[\sum_k m^I[k]\, s^I[k]\, \delta[n - kL]\right] * h[n] + j\left[\sum_k m^Q[k]\, s^Q[k]\, \delta[n - kL]\right] * h[n] \tag{8}$$

where $m^I[k]$ and $m^Q[k]$ are the multiplier coefficients that modulate the amplitude of the transmitted pulse components $s^I[k]$ and $s^Q[k]$, respectively.

Fig. 2(b) presents a scatter plot example of an 8-PSK constellation, when using polar and rectangular scaling. As can be observed, MM can seriously increase constellation symbols' sensitivity to noise. It can even cause some symbol's errors, as may happen for the case of higher-order non-constant amplitude constellations, unless there is some caution in choosing the factor MM m_n to apply to s_n. Hence, some common-sense simple rules are usually followed

- Avoid phase inversion by making $m_n > 0$;
- Keep, if possible, or at least minimize the decrease on the minimum distance between constellation symbols, by choosing $m_n \in]0, 1]$.

Phase inversion causes symbol errors and so m_n can't be negative. By restricting $m_n \in]0, 1]$, we only allow attenuation on the symbols to transmit and not their amplification. Amplification can be critical, especially in higher-order non-constant amplitude constellations. Here, in order to decrease some undesirable output peaks, it may be easy to amplify some inner symbols (small-amplitude symbols), in order to compensate the contribution of outer symbols (high-amplitude symbols), while attenuating, at the same time, the latter ones, thereby minimizing constellation's average power-loss due to MM. This minimization might even seem to be desirable based on the misleading conclusion that it would not affect the signal to noise ratio (SNR) at reception, and therefore system's BER performance. However, the described MM procedure would cause a dangerously close approximation of inner and outer symbols, decreasing too much the constellation's minimum distance, thus increasing constellation symbols' sensitivity to noise. As result, this would in fact, seriously degrade system's BER performance. This problem does not arise for constant amplitude constellations, wherefore amplification of symbols to transmit may be allowed [1], [2].

B.4 Synchronization and Detection

Synchronization, i.e., symbol period T_{SYMB} and carrier (frequency and phase) recovery, is also an important issue. Any estimation errors in these parameters may cause an additional BER degradation. When using MM, this is a problem when phase modulation on transmitted symbols is allowed (rectangular scaling). However, preferred MM solutions preserve phase, as is the case of the new MPMM presented in Section IV. In this case, several synchronization methods may be used successfully [16], [17], e.g., the ones used in [18]. The synchronization problem will therefore not be addressed, and BER results presented in this paper were obtained through simulation assuming coherent demodulation [19].

The increased sensibility to noise of the MM symbols may, however, require the use of improved detection schemes. In subsection IV-B, we propose the use of the expected average MM constellation (EAC) with success.

III. MAGNITUDE MODULATION: LUT-BASED APPROACH

Fig. 3 outlines a LUT-based implementation of the MM technique, as proposed in 2002 by Tomlinson *et al.* [3], [4]. MM coefficients are computed a priori by an iterative algorithm [5], [6], and stored in a LUT.

As already referred, the optimum MM factor to apply to each data pulse $s_n = s_n^I + j s_n^Q$, depends not only on s_n itself, but also on the D past and future symbol neighbors of s_n. Hence, MM coefficients m_n^I and m_n^Q that apply to s_n, are each one stored in

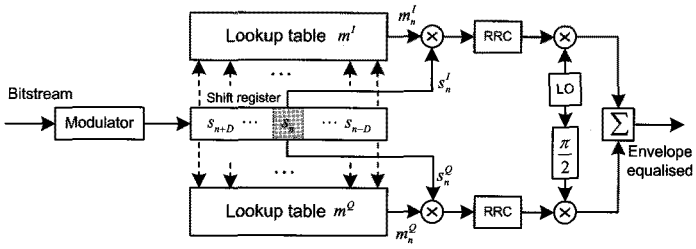

Fig. 3. LUT based magnitude modulation transmitter system.

a LUT, both at a position defined by the state

$$\mathbf{S_n} = [s_{n-D} \cdots s_{n-1}\ s_n\ s_{n+1} \cdots s_{n+D}]. \tag{9}$$

When performing polar scaling MM, the LUT-based magnitude modulation transmitter system present in Fig. 3 simplifies with only one LUT being required, since both s_n^I and s_n^Q are scaled by the same MM factor.

A. MM Look-Up-Table Computation

The iterative algorithm proposed by Tomlinson *et al.* [3], [4] for the a priori computation of MM factors, simply emulates a noiseless transmission of a band-limited (RRC filtered) signal, when peak-power control through clipping is used in the transmitter. The ratio of a received sample to the corresponding sent one, provides the value of the MM coefficient. However, that algorithm was targeted to constant amplitude constellations. As referred, we present an improved implementation of the LUT-MM technique, extending it to the more complex case of higher-order non-constant amplitude constellations.

Fig. 4 presents a discrete-time outline of the iterative algorithm we used for computing the MM coefficients. Different variations of this algorithm dictate the flow through the diagram. In a preferred embodiment, vectors

$$\mathbf{m}^I = \left[m^I_{-D} \cdots m^I_0 \cdots m^I_D\right], \tag{10}$$

$$\mathbf{m}^Q = \left[m^Q_{-D} \cdots m^Q_0 \cdots m^Q_D\right] \tag{11}$$

are initialized to all ones, and the algorithm iterates for each sequence of $N = 2D+1$ modulated symbols

$$\mathbf{s} = [s_{-D} \cdots s_0 \cdots s_D] \tag{12}$$

until it obtains a magnitude modulated sequence

$$\begin{aligned}\mathbf{a} = &\left[m^I_{-D}s^I_{-D} \cdots m^I_0 s^I_0 \cdots m^I_D s^I_D\right] \\ &+ j\left[m^Q_{-D}s^Q_{-D} \cdots m^Q_0 s^Q_0 \cdots m^Q_D s^Q_D\right]\end{aligned} \tag{13}$$

that guarantees that no limiting of the RRC filtered signal $v[n]$ (see Fig. 4) is necessary, i.e., $|v[n]|$ is upper bounded by

$$|v[n]| \leq A \tag{14}$$

where A is the normalized polar threshold, chosen in order to guarantee that the transmitter's HPA is not driven into saturation. Infinite loop situations may, however, happen when peak power of $v[n]$ falls to the close vicinity of the polar threshold A^2, but remains higher than A^2. Therefore, in order to increase algorithm's robustness, the limit condition (14) should be accompanied by monitoring the peak power of $v[n]$. The iterative procedure stops when $\max|v[n]|$ is in the close vicinity of A and doesn't decrease from one iteration to the next.

At the end of the iterative procedure, the m_0^I and m_0^Q values are stored in the LUT at the position defined by state $\mathbf{s}$ (i.e., mapped in the correspondent bit sequence).

Note, however, that during the iterative procedure all neighboring symbols of s_0 are also magnitude modulated (predistorted), and not only s_0, i.e., all elements of the $\mathbf{m}^I$ and $\mathbf{m}^Q$ vectors are updated. This assures that final values for m_0^I and m_0^Q will also take into consideration the magnitude modulation pre-distortion that neighboring symbols may suffer. Hence, applying the obtained MM coefficients m_0^I and m_0^Q to symbol s_0 when state $\mathbf{s}$ occurs in the transmitted stream, guarantees that minimum excursions above the threshold voltage A due to s_0 arise in the corresponding RRC output symbol interval of interest and its adjacent symbol intervals.

A.1 Filtering Finite Length Signals

Border problems for each state $\mathbf{s}$ due to RRC filtering of a finite length signal with zero padding [9], have a small impact on the accuracy of magnitude modulation values. During the iterative procedure, the MM factor of a border symbol (s_{-D} or s_D) may need to be changed in order to avoid clipping, due to lack of neighboring information. That change will be propagated along all inner symbols of the state. Hopefully, final coefficients can be refined by reduction the N LUT to a new one with $N' = N-2$ symbols per state, through a simple averaging operation.

Denote by $\mathcal{X}$ the set of constellation symbols of a M-ary constellation, $\mathbf{s}^{(N)}$ a N-tuple state defined by $N = 2D+1$ symbols as in (12) and let

$$\mathbf{m}_{\mathbf{s}^{(N)}} = \left(m^I_{\mathbf{s}^{(N)}}, m^Q_{\mathbf{s}^{(N)}}\right) \tag{15}$$

be the pair of MM coefficients resulting from applying the LUT-MM algorithm of Fig. 4 to state $\mathbf{s}^{(N)}$.

Let $N' = N-2$ and $\mathbf{s}^{(N')}$ be the state formed by the N' middle symbols of a state $\mathbf{s}^{(N)}$. There are M^2 states $\mathbf{s}^{(N)}_{i,j}$ that give rise to the same state $\mathbf{s}^{(N')}$, where

$$\mathbf{s}^{(N)}_{i,j} = \left[\ s_i\ \middle|\ \mathbf{s}^{(N')}\ \middle|\ s_j\ \right], \text{ with } s_i, s_j \in \mathcal{X}. \tag{16}$$

A pair of refined MM coefficients $\mathbf{m}_{\mathbf{s}^{(N')}}$ for state $\mathbf{s}^{(N')}$ can be obtained by performing an average over all $\mathbf{m}_{\mathbf{s}^{(N')}_{i,j}}$ with $i, j = 0, \cdots, M-1$, as follows

$$\mathbf{m}_{\mathbf{s}^{(N')}} = \frac{1}{M^2}\sum_{i=0}^{M-1}\sum_{j=0}^{M-1}\mathbf{m}_{\mathbf{s}^{(N')}_{i,j}}. \tag{17}$$

With this procedure we have succeeded to nearly eliminate the boundary influence. Referring to (9) note, however, that N should be large enough in order to the computed pair of MM factors that applies to a symbol s_n take into account not only the s_n itself, but also the influence of its neighbors. By applying this average procedure recursively, although the boundary influence vanishes on the computed MM coefficients and the LUT

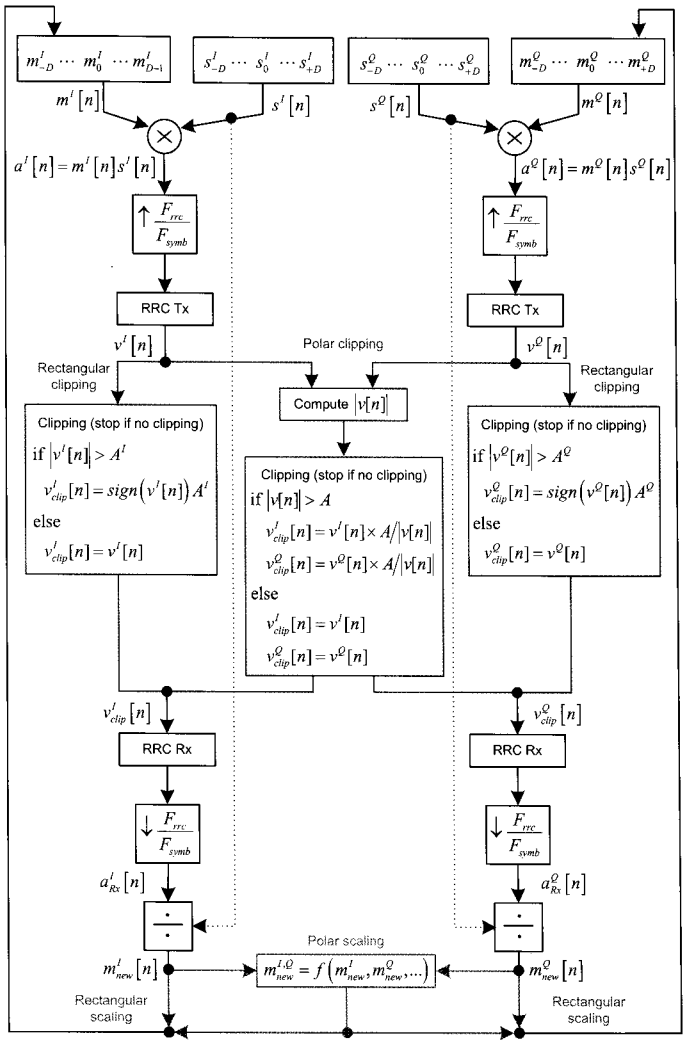

Fig. 4. Outline of the algorithm for computation of the LUTs of MM coefficients for a generic M-ary constellation.

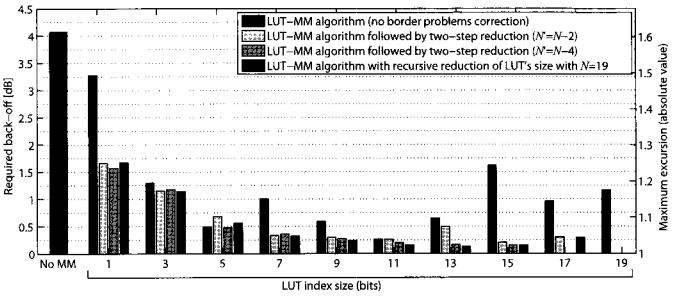

Fig. 5. Envelope maximum excursion and corresponding required back-off (dB) of a BPSK transmission with $\alpha = 0.35$ RRC pulse-shaping, as function of the LUT index size N.

memory size falls, the lack of information from s_n neighbors, causes a decrease of the MM envelope control performance. Fig. 5 shows these effects. It plots the envelope maximum excursion and the corresponding required back-off (dB) of a binary PSK (BPSK) transmission with $\alpha = 0.35$ RRC pulse-shaping, as function of the LUT index size (bits) when: Solo the LUT-MM algorithm from Fig. 4 is used; the LUT-MM algorithm is used followed by single-step and a two-step reduction through averaging of the LUT size; and recursively application of the averaging procedure. Excursion values are normalized assuming BPSK symbols $s_n = \pm 1$ and $G_{\mathrm{RRC}} = 1$. It is clear the reduction in the required back-off as function of N (LUT index size), with the use of the MM technique after elimination of the boundary influence through (17).

B. LUT-MM Improvements to Handle Generic M-ary Constellations

Fig. 4 shows four different algorithm approaches for the computation of magnitude modulation tables,

- Rectangular clipping-rectangular scaling (RC-RS);
- Rectangular clipping-polar scaling (RC-PS);
- Polar clipping-rectangular scaling (PC-RS);
- Polar clipping-polar scaling (PC-PS).

B.1 Clipping

According to Fig. 4, envelope clipping after RRC filtering at transmitter can be performed by separately limiting the v_n^I and v_n^Q components (rectangular clipping) or by rescaling them together, when the envelope's magnitude $|v[n]| > A$ (polar clipping).

In [4], the authors chose the component clipping levels as

$$A^I = A^Q = \frac{A}{\sqrt{2}} \tag{18}$$

for the rectangular clipping case, since they were dealing with constant amplitude constellations.

For non-constant amplitude modulations different values must be set for A^I and A^Q according to the constellation design. Denoting the M symbols of an M-ary constellation by X_n, with $n = 0, \cdots, M-1$, we can guarantee that $|x[n]| \leq A$ in the separate limiting case of v_n^I and v_n^Q by setting

$$A^I = \max_{n=0,\cdots,M-1} |\Re(X_n)|, \tag{19}$$

$$A^Q = \max_{n=0,\cdots,M-1} |\Im(X_n)| \tag{20}$$

where $\Re(X_n)$ and $\Im(X_n)$ denotes the real and imaginary parts of $X_n \in \mathbb{C}$, and, thus,

$$A = \max_{n=0,\cdots,M-1} |X_n| = \sqrt{(A^I)^2 + (A^Q)^2}. \tag{21}$$

These conditions are simply an extension of the limits defined for constant amplitude modulations. However, they are very restrictive and MM coefficients computed according to them will lower too much the power of the transmitted signal, leading to a decrease on the BER performance. For M-ary non-constant amplitude modulations and equiprobable symbols, the probability that of one of the signal components, v_n^I or v_n^Q, violates (19) and (20) while $|x[n]| \leq A$, is very high, especially, if the majority of constellation symbols have amplitude lower than A. Therefore, the clipping limits should take into account the average energy of both I and Q components according to

$$A^I = \sqrt{A^2 - E\left\{|\Im(X_n)|^2\right\}}, \tag{22}$$

$$A^Q = \sqrt{A^2 - E\left\{|\Re(X_n)|^2\right\}} \tag{23}$$

Table 2. LUTs size for different MM algorithm approaches.

	RC-RS case	Remaining cases
Table m^I:	$2^{b_I \times N}$	$M^N = 2^{(b_I+b_Q)\times N} = 2^{b_I \times N} \times 2^{b_Q \times N}$
Table m^Q:	$2^{b_Q \times N}$	$M^N = 2^{(b_I+b_Q)\times N}$

where $E\{X_n\}$ is the expected value of a random variable X_n.

These new limits, don't guarantee the condition $|x[n]| \leq A$ at every instant. In fact, at worst case conditions a maximum excursion of

$$\sqrt{(A^I)^2 + (A^Q)^2} > A \tag{24}$$

may be observed, however, their probability is too low when compared to the conditions expressed by (19) and (20).

B.2 Scaling

In order to avoid phase modulation, m^I and m^Q can be forced to be equal, $m^{I,Q}$ (polar scaling). In [4], it was proposed to use the arithmetic mean, i.e., in Fig. 4, $m^{I,Q}_{\text{new}}$ was defined as

$$m^{I,Q}_{\text{new}} \triangleq \frac{m^I_{\text{new}} + m^Q_{\text{new}}}{2} \tag{25}$$

for the QPSK case. For higher order constellations, whose symbols have unequal amplitude components, we define a new averaging function. The idea is to preserve the power of the MM symbol when restricting $m^I = m^Q$, when compared to the power of the symbol obtained with the use of rectangular scaling. Hence, $m^{I,Q}_{\text{new}}$ is computed as

$$m^{I,Q}_{\text{new}} \triangleq \sqrt{\frac{(m^I_{\text{new}} s^I)^2 + (m^Q_{\text{new}} s^Q)^2}{(s^I)^2 + (s^Q)^2}}. \tag{26}$$

C. LUT-MM Complexity Discussion and Algorithm's Optimization

Computational complexity and LUTs size (hence, storage requirements) depend on the different clipping and scaling approaches that can be followed, the shape and dimension of the considered M-ary constellation and the shift register length, $N = 2D + 1$ (Fig. 4).

Denote by b_I and b_Q the number of bits associated with I and Q components of the constellation symbols. The number of constellation symbols is

$$M = 2^{b_I + b_Q} \tag{27}$$

and, for square constellations,

$$b_I = b_Q = \frac{\sqrt{M}}{2}. \tag{28}$$

By observing Fig. 4, it is easy to conclude that for the RC-RS case, the two computation branches are completely separated, with m^I_0 and m^I_0 being function only of $\mathbf{s}^I = \Re(\mathbf{s})$ and $\mathbf{s}^Q = \Im(\mathbf{s})$, respectively. For the remaining cases, there are interconnections between the two branches and, so m^I_0 and m^Q_0 values depend on the whole vector s. These correspond to a huge difference in the LUT's size between the RC-RS approach and the remaining cases as it is show in Table 2.

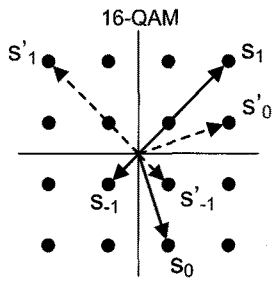

Fig. 6. Equivalent $\frac{n\pi}{2}$ rotated state of $\mathbf{s} = [s_{-1}\ s_0\ s_1]$.

If we consider a square constellation, the complexity of RC-RS case can even be more simplified. The set of combinations $\mathbf{s}^I$ and $\mathbf{s}^Q$ to compute both LUTs for m^I_0 and m^Q_0 are equal. Thus, only one branch of the diagram (Fig. 4) needs to be run so the magnitude modulation system (Fig. 3) can be implemented with a single LUT.

C.1 Exploring Constellation Symmetry

The main facing problem of extending the method to a higher order M-ary constellation, is the high number of constellation. symbols with non-constant amplitude which leads to a huge number of combinations to be considered, even for a system with small memory. Hopefully, the considered M-ary constellations are usually symmetric with respect to both, real and imaginary axis.

As stated before, let $\mathcal{X}$ denote the set of constellation symbols of a M-ary constellation, and $\mathcal{X}^{n^{th}}$ the subset of the ones belonging to the n^{th} quadrant. For the case of a symmetric constellation, any state s defined as in (12), whose central symbol $s_0 \notin \mathcal{X}^{1^{st}}$, i.e.,

$$\angle s_0 = \alpha + n\frac{\pi}{2}, \text{ with } \alpha \in \angle\left(\mathcal{X}^{1^{st}}\right),\ n \in \{1,2,3\} \tag{29}$$

can be transformed to an equivalent state

$$\mathbf{s}' = \left[s'_{-D} \cdots s'_0 \cdots s'_D\right] = e^{-jn\frac{\pi}{2}}\mathbf{s} \tag{30}$$

where $s'_0 \in \mathcal{X}^{1^{st}}$ and $\angle s'_0 = \alpha$.

Fig. 6 presents an example of a 16-QAM equivalent symbol state through the rotation procedure (30).

Based on the following proposition [5], only states whose central symbol belongs to $\mathcal{X}^{1^{st}}$ need to be computed and stored in a LUT. This leads to a reduction on the number of states to be considered by a factor of 2 for RC-RS case and by a factor of 4 for the remaining LUT-MM approaches.

Proposition 1: For rotated states $\mathbf{s}' = e^{-jn\frac{\pi}{2}}\mathbf{s}$ (with $\mathbf{s}' \in \mathcal{X}^{1^{st}}$ and $\mathbf{s} \notin \mathcal{X}^{1^{st}}$), magnitude modulation factors are related by

$$s_0 \in \left\{\mathcal{X}^{2^{nd}}, \mathcal{X}^{4^{th}}\right\} \quad \Rightarrow \quad (m^I, m^Q) = (m'^Q, m'^I) \tag{31}$$

$$s_0 \in \mathcal{X}^{3^{rd}} \quad \Rightarrow \quad (m^I, m^Q) = (m'^I, m'^Q). \tag{32}$$

C.2 Exploring RRC symmetry

RRC digital filters of Figs. 3 and 4 are typically chosen to be linear phase which allows to further reduce the number of combinations to be computed according to proposition 2 [5].

Table 3. Computation complexity and LUTs storage requirements considering constellation and RRC symmetries.

	RC-RS case	Remaining cases
Table m^I:	$\frac{1}{4}\left(2^{b_I N}+2^{b_I\left(\frac{N+1}{2}\right)}\right)$	$\frac{1}{8}\left(M^N+M^{\frac{N+1}{2}}\right)$
Table m^Q:	$\frac{1}{4}\left(2^{b_Q N}+2^{b_Q\left(\frac{N+1}{2}\right)}\right)$	$\frac{1}{8}\left(M^N+M^{\frac{N+1}{2}}\right)$

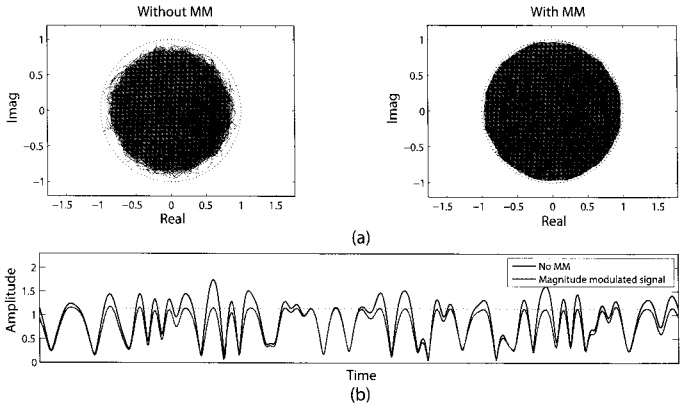

Fig. 7. Sample of a $\alpha = 0.35$ RRC filtered 16-APSK signal with and without MM: (a) State space diagram (under the constraint of unitary maximum transmitted power) and (b) sample of a magnitude modulated 16-APSK signal.

Proposition 2: Let $\mathbf{s_r}$ be the time reversal of state $\mathbf{s}$. For linear phase filters with even impulse response

$$h_{\text{rrc}}[n] = h_{\text{rrc}}[-n] \tag{33}$$

both states, $\mathbf{s_r}$ and $\mathbf{s}$, have the same magnitude modulation coefficients.

Proposition 2 allows a reduction to almost a half in the number of states to be computed (there are $M^{\frac{N-1}{2}}$ states for which $\mathbf{s_r} = \mathbf{s}$).

Exploring both, constellation symmetries and RRC linear phase, LUT-MM algorithm complexity and LUT storage requirements are reduced almost 4 times for the RC-RS case, and 8 times for the remaining cases, as presented in Table 3.

D. Simulation Results

This section presents some experimental results showing to be possible to extend the MM technique to constellations with $M = 16$. A 16-APSK constellation with $\gamma = 3.15$, taken from DVB-S2 standard [10], and a 16-QAM constellation are considered. Both constellations are normalized, i.e., with average energy per transmitted symbol equal to one.

Fig. 7 illustrates a sample of a $\alpha = 0.35$ RRC filtered 16-APSK signal with and without MM. The method clearly limits the maximum peak power. Envelope excursions above maximum amplitude A, are smoothed scaled without clipping, as desired. In practice, with a restriction on the maximum admissible power at HPA input to prevent HPA output's saturation, the MM method allows the transmission of a much higher power to the channel as can be observed in Fig. 7(a) at right, where the outer constellation symbols are closer to the limit circle.

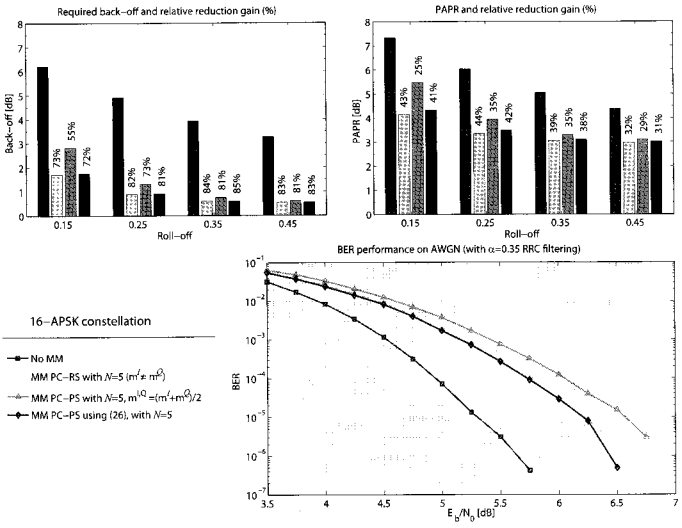

Fig. 8. BER performance, PAPR, and back-off gains of several MM approaches for a 16-APSK RRC filtered signal.

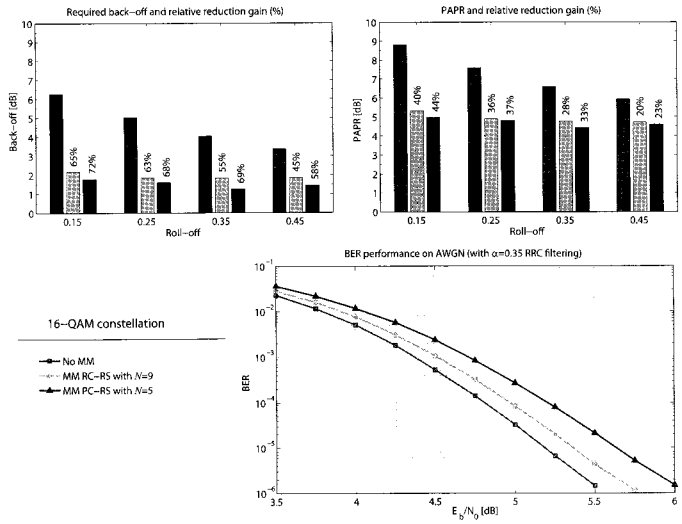

Fig. 9. BER performance, PAPR, and back-off gains of several MM approaches for a 16-QAM RRC filtered signal.

For the polar scaling case, the new proposed function (26) is evaluated against (25) previously used [4]. Results presented in Fig. 8, consider a system memory of $N = 5$ and polar clipping, for the 16-APSK constellation. Performance is also evaluated in terms of BER for the additive white Gaussian noise (AWGN) channel assuming linear transmission (ideal HPA operation) of a $\alpha = 0.35$ RRC pulse shaped signal. Forward error correcting coding was used, considering the $(576, 288)$ low-density parity-check code (LDPC) [20] defined in the Wimax 802.16e standard [21]. The logarithmic sum-product algorithm algorithm (LSPA) [22], following a horizontal schedule [23] approach, was used on decoding.

Even for a small memory system, e.g., $N = 5$, the LUT-MM method allows a considerable reduction of about 80% on the required back-off. PAPR reduction in dB is lower than the back-off reduction as desired, i.e., the expected decrease on transmitted average power due to the MM procedure is much lower than the desired reduction on output peak power, and so a small

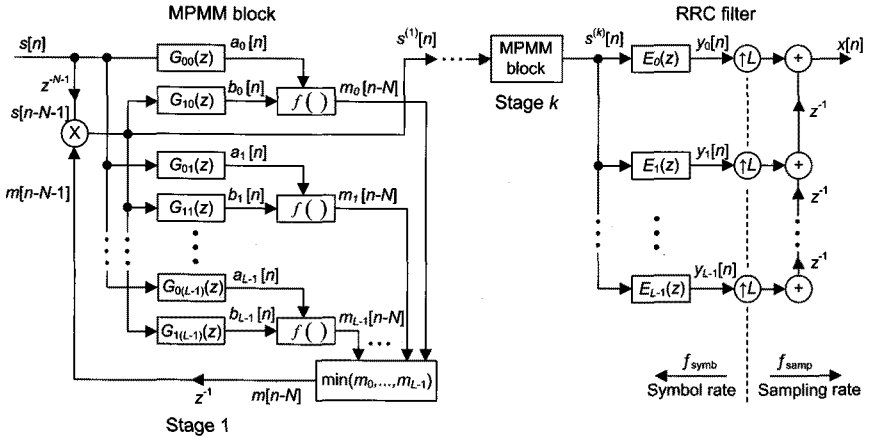

Fig. 10. Multistage polyphase MM scheme for controlling the signals excursion at the RRC output, followed by the RRC filter block.

penalty on BER performance should be expected. This is confirmed by the BER results. The short LDPC code efficiently compensates the increased sensitivity to noise due to the MM technique, with the MM system performing only 1 dB away (at BER $= 10^{-6}$) with comparison to the linear transmission non-MM case. The overall back-off gain (back-off gain minus BER loss) is more than 2.5 dB at BER$= 10^{-6}$, which is a significant improvement.

Considering function (26), it presents no loss when compared to the LUT-MM method under the rectangular scaling approach (i.e., $m^I \neq m^Q$), with the major advantage of not introducing phase distortion on transmitted symbols that could cause synchronization problems on reception. In the typical range of interest, $\alpha \in [0.15, 0.35]$, the back-off gain is significantly better than the one obtained by the average function (25) [4]. Fig. 8 shows also that even at $\alpha = 0.35$, where both functions present similar back-off gains, a further gain of about 0.4 dB is obtained at BER $= 10^{-5}$.

We also evaluated the advantage of using a RC-RS approach when separation can be performed on the set of bits that map to I and Q symbol's components. Results for the 16-QAM modulation are presented in Fig. 9 for the RC-RS and PC-RS approaches. Here, both methods are compared within a similar LUT size criterion. Performance considering a system memory of $N = 9$ for the RC-RS case, is compared to the PC-RS with $N = 5$.

As desired, both methods show a significant reduction of the back-off (60% – 70% range). Although for PC-RS with $N = 5$ the performance is slightly better than for RC-RS with $N = 9$, there is no flexibility for changing N due to the problematic huge LUT size. In addition, in terms of BER performance RC-RS performs better than PC-RS, only 0.2 dB apart from the non-MM system at BER$= 10^{-6}$, which also confirms the efficiency of the LUT-MM method. The total back-off gain (back-off gain minus BER loss) is then 2 dB for RC-RS, and 2.3 dB for PC-RS.

IV. MULTISTAGE POLYPHASE MAGNITUDE MODULATION

The polyphase decomposition [9], [24] of the pulse shaping filter (Fig. 1), $H(z)$, is behind the idea of a LUT-less MM approach. In Fig. 10, we present a k-stage MPMM system, followed by the polyphase representation of the RRC filter. Each stage incrementally adjusts the symbols amplitudes, in order to control the excursion at the RRCs output.

A. The MPMM Principle

Lets assume, without loss of generalization, a type I linear phase FIR RRC filter whose impulse response spreads over $2N + 1$ symbols and which is given by

$$H(z) = \sum_{n=0}^{2NL} h[n]\, z^{-n} \quad \text{with} \quad h\,[n] = h\,[2NL - n] \tag{34}$$

where the over-sampling L is even. Similar developments for a type II filter or an odd L can, easily, be inferred.

Pulse shaping can be performed at symbol rate using the polyphase scheme [9], [24] displayed in Fig. 10, with

$$E_i(z) = \sum_{n=0}^{2N} e_i[n]\, z^{-n} = \sum_{n=0}^{2N} h[nL + i + \lambda]\, z^{-n} \tag{35}$$

considering the required zero padding as shown in Fig. 13 and where $\lambda \in \mathbb{Z}$ is the filter decomposition phase offset.

The output $x[n]$ is given by one of the polyphase filters' output, at instant $n_0 = \lfloor n/L \rfloor$, since

$$x[n] = y_{(n \bmod L)}\left[\lfloor n/L \rfloor\right]. \tag{36}$$

All outputs $y[n_0]$, with $i = 0, \cdots, L-1$, depend on the same set of inputs symbols $s[k]$, with $k = n_0 - 2N, \cdots, n_0$, since

$$y_i\,[n] = \sum_{k=0}^{2N} e_i[k]\, s[n-k]. \tag{37}$$

The MPMM principle consists in computing the best MM coefficient $m[n_0]$ to apply into symbol $s[n_0]$, so as to guarantee that

$$|x[n]| \leq A \tag{38}$$

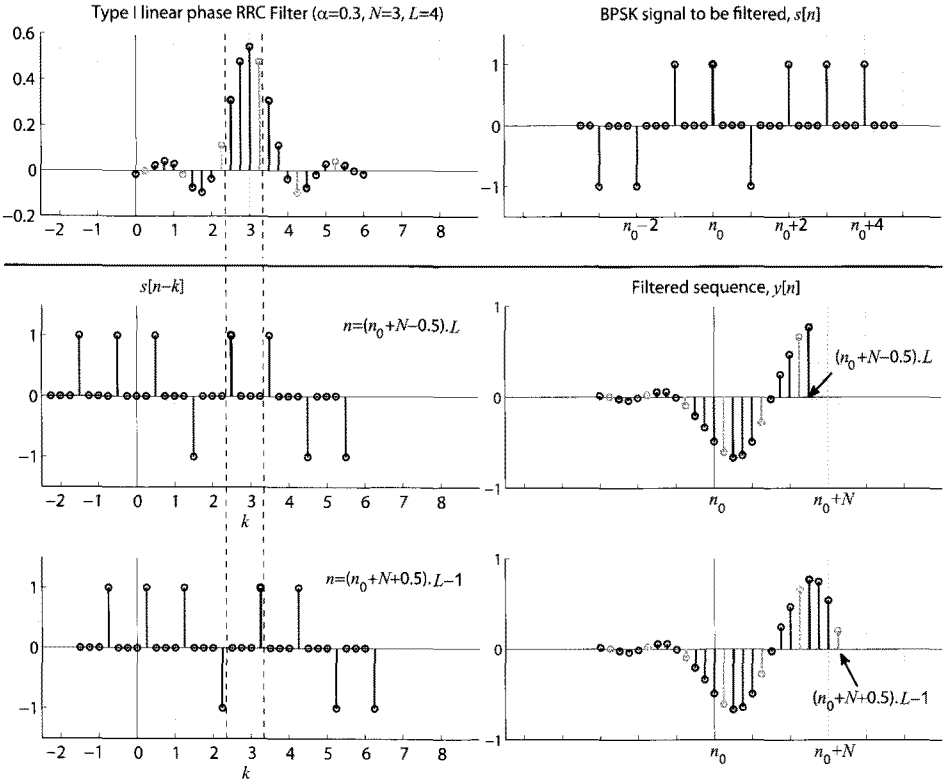

Fig. 11. Controlling the output around sample n_0+N, within a range of L samples.

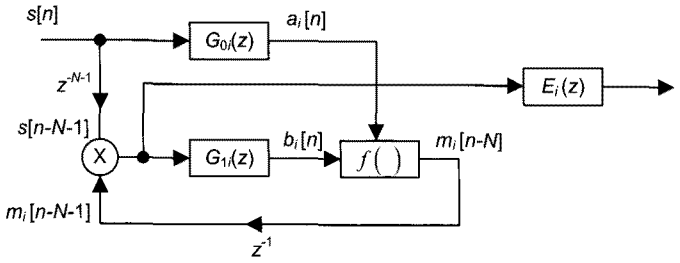

Fig. 12. Detailed MPMM's branch.

where A is the specified polar threshold.

Computation of $m[n_0]$ takes into account the RRC output samples, at those sampling instants, for which $s[n_0]$ most contributes. Once the energy of the impulse response $h[n]$ is centered around sample NL, $s[n_0]$ is, according to (36) and (37), the most relevant symbol to the RRC output excursion, $x[n]$, during the interval $[(n_0+N-0.5)L, (n_0+N+0.5)L]$, as shown in Fig. 11. Those samples can be observed at the same time instant at the output of polyphase filters' bank, $E_i(z)$ with $i=0,\cdots,L-1$, when considering a polyphase decomposition with offset $\lambda=-L/2$.

Based on this premise, setting $\lambda=-L/2$, we have developed the system of Fig. 10, that adjusts the amplitude of symbol $s[n_0]$ in order to control the output excursion of all polyphase filters $E_i(z)$ at sampling instant n_0+N (Fig. 11), so as to guarantee that

$$|y_i[n_0+N]| \leq A. \tag{39}$$

The impulse responses of FIR filters $G_{0i}(z)$ and $G_{1i}(z)$ are obtained directly from $e_i[n]$ as sketched in Fig. 13, thus being defined as

$$g_{0i}[n] = \begin{cases} e_i[n], & 0 \leq n \leq N \\ 0, & \text{otherwise} \end{cases} \tag{40}$$

$$g_{1i}[n] = \begin{cases} e_i[n+N+1], & 0 \leq n \leq N-1 \\ 0, & \text{otherwise.} \end{cases} \tag{41}$$

For a better understanding and without loss of generality, we will focus our attention in Fig. 12, which depicts a single branch of the MPMM system. When magnitude modulation is used, (37) is written as

$$y_i[n] = \sum_{k=0}^{2N} e_i[k]\, m_i[n-k]\, s[n-k] \tag{42}$$

where $m_i[n]$ is the sequence of MM coefficients which control the output peak power of polyphase filter $E_i(z)$.

Basically, the system tries to anticipate the output of $E_i(z)$ at each instant n_0+N and, accordingly, it computes the MM factor $m_i[n_0]$ to apply into $s[n_0]$, the input sample that most contributes to the output $y_i[n_0+N]$. Each MPMM stage system introduces, therefore, a small delay of NT_{SYMB} during transmission. When computing $m_i[n_0]$, coefficients $m_i[n_0-k]$, with $k=1,\cdots,N$, are already known (past symbols relative to $s[n_0]$). However, nothing is known about the MM values that will magnitude modulate symbols $s[n_0-q]$, with $q=-N,\cdots,-1$ (future symbols relative to $s[n_0]$). In order to avoid excessive time variation of the average power of the signal after pulse shaping, we assume that future symbols should be MM as

$$m_i[n_0-q] \simeq m_i[n_0], \quad \text{for} \quad q=-N,\cdots,-1. \tag{43}$$

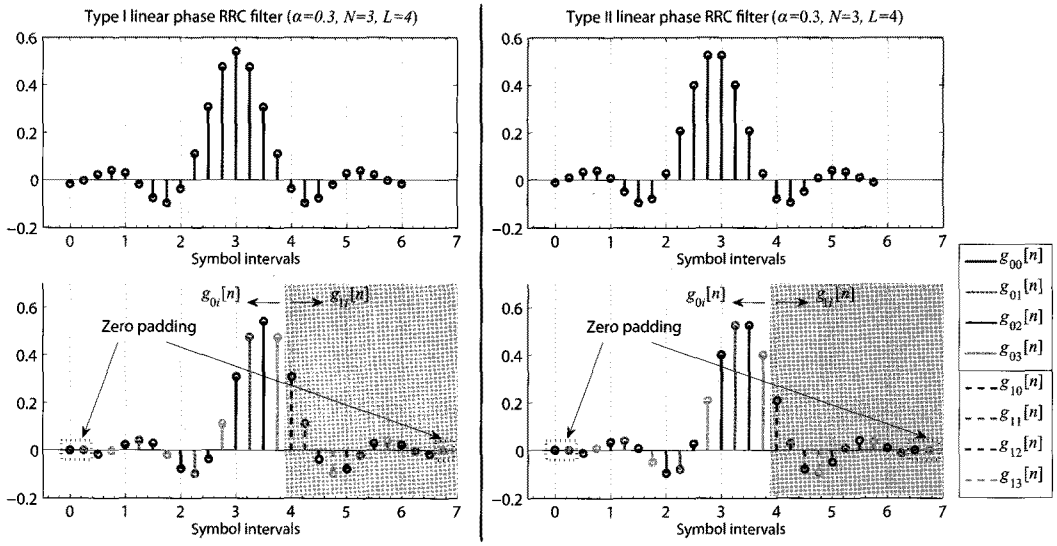

Fig. 13. MPMM component filters, $g_{0x}[n]$ and $g_{1x}[n]$, for polyphase decomposition with phase-offset, $\lambda = -L/2$.

Considering equality in (43), a non-negative $f(\cdot)$ function (see Appendix) is defined so as to guarantee (46). The procedure just described computes the MM factor $m_i[n]$, that multiplies each symbol $s[n]$, in order to limit the excursion at the output of a particular filter $E_i(z)$. However, $m[n]$ has to be unique and has to guarantee that $|y_i[n]| \leq A$ at the output of all filters $E_i(z)$ (with $i = 0, \cdots, L-1$). We have solved this problem by multiplying each symbol $s[n]$ by the most restricted factor, i.e., by computing

$$m[n] = \min_{i=0,\cdots,L-1} (m_i[n]). \tag{44}$$

However, a further improvement on $m[n]$ has to be done, since the equality condition in (43) is only assumed when computing $m[n_0]$. When MM coefficient $m[n_0+1]$ is greater than $m[n_0]$, condition $|y_i[n_0+N]| \leq A$ doesn't hold. Nevertheless, since symbol $s[n_0+1]$ is more relevant to output $y_i[n_0+N+1]$ than $y_i[n_0+N]$, there must be a compromise for $m[n_0+1]$ that doesn't decrease $y_i[n_0+N+1]$ too much (which is undesirable) and still guarantees that restriction $|y_i[n_0+N]| \leq A$ is only slightly violated. A simple procedure to accomplish this was found by using the following time variant filter

$$m[n+1] > m[n] \Rightarrow m'[n+1] = \frac{m[n+1]+m[n]}{2}. \tag{45}$$

A.1 Multistage PMM

One of the major advantages of the proposed polyphase MM scheme, is the fact that the system design depends only on the RRC impulse response. There is no restriction on the input type signal, which makes this new proposed technique independent of the constellation being used. The system adjusts the amplitude of the input symbols independently of its type, which means that this procedure can also be applied to a sequence that was already processed by MM, in order to further adjust its symbols and to achieve a better control of its output excursion. The back-off to apply to an input signal can therefore become almost negligible by using a cascade of a few MPMM blocks similar to that represented in Fig. 10.

The MPMM technique doesn't present a notable complexity (very large-scale integration (VLSI) or digital signal processing (DSP)) to the transmitter system, since it only corresponds to a basic FIR filtering system. Instead, LUT-MM method requires a ROM dimension given in Table 3, which may become prohibitive for large M-ary constellations.

B. MPMM Simulation Results

The MPMM technique was evaluated for different M-ary constellations. Unlike the LUT-MM approach, there is no restriction in applying the method to constellations with $M \geq 16$. We choose to present some of the obtained results through simulation for the 8-PSK, 16-APSK (with $\gamma_1 = 3.15$), and 32-APSK (with $\gamma_1 = 2.84$ and $\gamma_2 = 5.27$) [10], constellations that find particular application in satellite communications, mainly due to their low $\text{PAPR}_{\text{Const}}$. Results for the normalized 16-QAM constellation are also reported and its performance under MPMM is evaluated and compared with 16-APSK.

Simulations were conducted for a pulse-shaping filter with different values of roll-off in the range $[0.1, 0.5]$. The results for the demanding case of sharp roll-off RRC filtering with $\alpha = 0.2$ used in DVB-S2 [10] are depicted in Figs. 14–17.

Fig. 14 shows the reduction on the required back-off obtained with the MPMM method, and the PAPR of the MM signal. For a better comparison with the LUT-MM technique, the best results (among the different proposed approaches) for a memory size of $N = 5$ are included in the figure. In addition, we included the case of RRC filtering with $\alpha = 0.35$ for comparison with Figs. 8 and 9.

MPMM clearly outperforms LUT-MM technique. With just 1-stage MPMM the need to use back-off is reduced more than 88%. When considering 2-stages, it almost vanishes with reduction gains always above 95% (result obtained for the different tested constellations when considering an even more demanding case of RRC filtering with $\alpha = 0.1$).

Fig. 14 also shows that MPMM performs identically for the

$$|y_i[n_0+N]| \le A \Leftrightarrow \left|\sum_{k=0}^{2N} e_i[k]\, m_i[n_0+N-k]\, s[n_0+N-k]\right| \le A \Leftrightarrow$$

$$\Leftrightarrow \left|m_i[n_0]\sum_{k=0}^{N} e_i[k]\, s[n_0+N-k] + \sum_{k=N+1}^{2N} e_i[k]\, m_i[n_0+N-k]\, s[n_0+N-k]\right| \le A$$

$$\Leftrightarrow \Bigg|m_i[n_0]\underbrace{\sum_{k=0}^{N} g_{0i}[k]\, s[n_0+N-k]}_{a_i[n_0] \text{ according to Fig. 12}} + \underbrace{\sum_{k=0}^{N-1} g_{1i}[k]\, m_i[n_0-k-1]\, s[n_0-k-1]}_{b_i[n_0] \text{ according to Fig. 12}}\Bigg| \le A$$

$$\Leftrightarrow |m_i[n_0]\, a_i[n_0+N] + b_i[n_0+N]| \le A \quad \Rightarrow \quad m_i[n_0] = f(A, a_i[n_0+N], b_i[n_0+N]) \qquad (46)$$

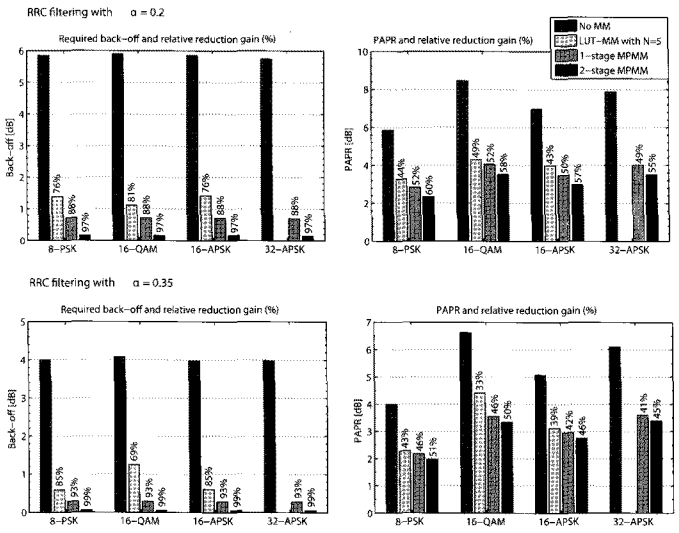

Fig. 14. PAPR and back-off gains of MPMM applied to different constellations when performing bandwidth pulse shaping with $\alpha = 0.2$ and 0.35.

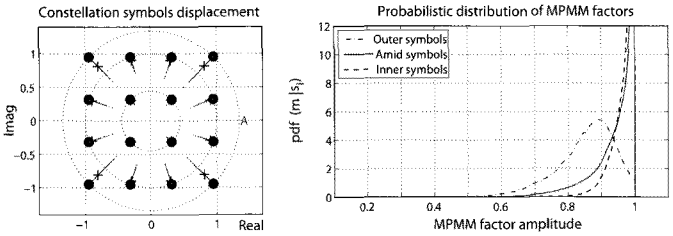

Fig. 15. MPMM method applied to 16-QAM transmission with $\alpha = 0.2$ RRC filtering. Scatter plot and pdf distributions of the symbols' displacement considering a 2-stage system (• original symbol's positions; + MPMM symbols' average positions).

different constellations. This behavior was expectable, since maximum excursion above the desired limit A, is mainly due to outer-circle symbol combinations. Consequently, the system behavior should be the same in such cases, as verified. This important fact demonstrates that this technique is independent of the modulation being used, as previously claimed.

As desired, PAPR reduction is lower than back-off reduction, i.e., the expected decrease on transmitted average power due to the MM procedure is much lower than the desired reduction on output peak power as was recently analytically shown [25]. This small decrease of the average transmitted power due to MM, justifies the small penalty on BER.

B.1 BER Performance

In subsection III-D, when analyzing the BER performance of the LUT-MM technique, we assumed that the receiver is MM's blind, i.e., the receiver operates normally as if no MM was previously applied at the transmitter's side. Due to the distortion made by the MM procedure to the transmitted symbols, some increased sensibility to noise was observed. Hopefully, this loss was far overcompensated by the gain obtained in the required back-off.

MPMM performs a fine control of signal's envelope excursion and so an aggravation on the sensibility to noise should be expected. This sensibility to noise depends also on the constellation geometry, which is easily understandable by observing the constellation symbolsÕ displacement due to MPMM, as shown in Fig. 15 for the 16-QAM case. Non-constant amplitude constellations with low PAPR or with aligned symbols (same phase) are more prone to MM noise. However, it doesn't introduce distortion on the phase of transmitted symbols and so receiver synchronization shouldn't be an issue [16], [18] (no further degradation on BER is to be expected).

Soft-decoding estimates should, therefore, take into account the symbol displacement statistics due to MM. A simply way to accomplish this, without changing the existing receivers, is to compute those estimates based on the EAC [7], [25]. The average position of constellation symbol s_i from an M-ary constellation $\mathcal{X}$, after being MM can thus be computed as

$$\overline{s}_{i_{\text{MM}}} = s_i E\{m\,|s_i\} = s_i \int_0^1 m\, p(m\,|s_i)\, dm \qquad (47)$$

where $p\,(m\,|s_i)$ is the conditional probability density function (pdf) of a MM factor m, given the constellation symbol $s_i \in \mathcal{X}$. It has been shown [25] that $p(m\,|s_i)$ follows a beta distribution, i.e.,

$$p(m|s_i) = \frac{\Gamma(\alpha+\beta)}{\Gamma(\alpha)\,\Gamma(\beta)} m^{\alpha-1}\,(1-m)^{\beta-1} \qquad (48)$$

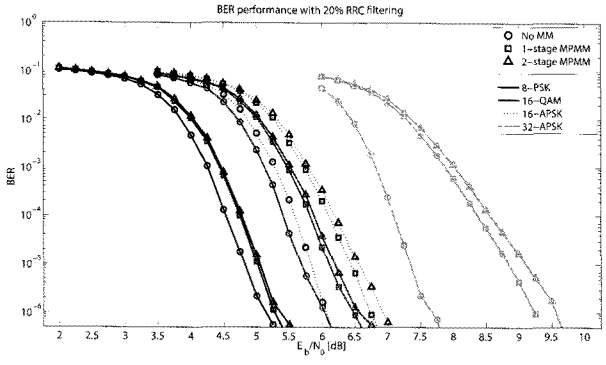

Fig. 16. Soft-decoding BER performance of MPMM applied to different constellations when performing bandwidth pulse shaping with $\alpha = 0.2$, and FEC system based on the $(1248, 832)$ LDPC code [21].

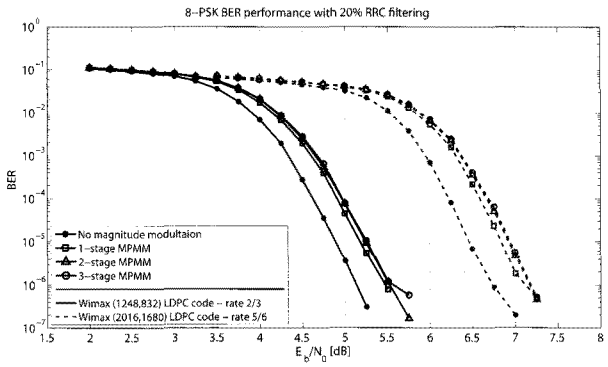

Fig. 17. Soft-decoding BER performance of MPMM applied to 8-PSK, RRC filtered with $\alpha = 0.2$, when using the $(1248, 832)$ and $(2016, 1680)$ LDPC codes [21].

where $\Gamma(\alpha) = \int_0^\infty x^{\alpha-1}e^{-x}dx$ represents the gamma function. In fact, due to constellation and RRC symmetry properties, the pdf of m is only conditioned on $|s_i|$ and so (48) is the same for all the symbols in $\mathcal{X}$ having the same magnitude. Parameters, α and β, have been tabulated for different constellations and RRC's roll-offs in [25].

The EAC, $\overline{\mathcal{X}}_{\text{MM}}$, is simply the set of all symbols $\overline{s}_{i_{\text{MM}}}$, with $i = 0, \cdots, M-1$, computed according with (47). This set can be easily obtained a priori through simulation and so be known by the receiver. As an example, in Fig. 15 we plot the MPMM EAC constellation for 16-QAM transmission with $\alpha = 0.2$ RRC filtering, and the pdf of the MM factors.

Fig. 16 illustrates the BER performance of the MPMM scheme when using the EAC in the computation of initial soft decoding estimates. Remaining conditions are the same as considered in subsection III-D, i.e., transmission over the linear AWGN channel and a FEC system based on the (1248, 832) LDPC Wimax 802.16e code [21], with horizontal scheduled LSPA decoding [22], [23].

Although, the selected code rate is $2/3$, we observe that it efficiently compensates the increased noise sensibility due to MM. Even for the worst scenario, the 32-APSK with 2-stage MPMM, the BER performance loss with respect to non-MM case at BER$= 10^{-6}$ is only 1.8 dB. Since the back-off reduction is 5.6 dB, the power efficiency of the system is improved by more than 3.8 dB. For the 8-PSK case, the overall back-off gain reaches 5.4 dB.

Comparing 16-QAM and 16-APSK constellations, we observe that the latter one is more prone to MM noise distortion. In this case, the two sets of constant-amplitude symbol amplitudes that form the constellation, contain outer symbols aligned with inner symbols, and under MM a dangerously close approximation occurs between them. Hence, the practical advantage of using 16-APSK, due its low $\text{PAPR}_{\text{Const}}$, vanishes when using MM, with both, 16-QAM and 16-PSK, performing similarly. Although, 16-QAM still shows a slightly higher PAPR when using MPMM, this is compensated by a better BER performance.

Fig. 17 illustrates the BER performance for 8-PSK also with a $(2016, 1680)$ LDPC Wimax 802.16e code [21]. By providing good estimates based on the EAC to the soft-decoder, although using different codes, the performance of the MPMM technique is similar, i.e., for a code with weaker error correction capabilities we don't observe a notorious degradation in BER performance due to MM. Hence the EAC and system's FEC can efficiently compensate the increased sensitivity to noise resulting from MM, as claimed before. This means that no additional error control protection is required, so the information rate and the quality of service links are preserved.

V. CONCLUSION

In this paper, we have performed a detailed description of the MM concept and its recent developments, for single-carrier VSAT's transmitter systems. The LUT-MM and MPMM approaches were discussed in depth. We show that MM is a suitable power back-off reduction technique in the referred context.

APPENDIX

Given $a, b \in \mathbb{C}$ and $A \in \mathbb{R}^+$, we want to find the maximum value for $m \in [0, 1]$ that satisfies

$$|ma + b| \leq A \tag{49}$$

- Case $|ma + b| \leq A$,

$$m = 1; \tag{50}$$

- Case $|ma + b| > A$ condition (49) is satisfied with equality when

$$\begin{aligned} |m\,a+b| = A &\Leftrightarrow (m\,a + b)(m\,a + b)^* = A^2 \\ &\Leftrightarrow |a|^2 m^2 + 2\text{Re}\{ab^*\}\, m + |b|^2 - A^2 = 0. \end{aligned} \tag{51}$$

An $\mathbb{R}^+$ solution for the quadratic equation in m exists if $|b| < A$. Due to the asymmetrical partition of polyphase filter $E_i(z)$ in filters given by (40) and (40), this condition is always verified in practice. Combining (50) and (51) we define a non-negative function given by

$$f(A, a, b) = \begin{cases} 1, & |a + b| \leq A \\ \dfrac{-\Re\{ab^*\} + \sqrt{\Re\{ab^*\}^2 - |a|^2(|b|^2 - A^2)}}{|a|^2}, & |a + b| > A. \end{cases} \tag{52}$$

REFERENCES

[1] S. Miller and R. O'Dea, "Radio with peak power and bandwidth efficient modulation," U.S. Patent 5 621 762, 1997.

[2] ——, "Peak power and bandwidth efficient linear modulation," *IEEE Trans. Commun.*, vol. 46, no. 12, pp. 1639–1648, Dec. 1998.

[3] A. Tomlinson, A. Ambroze, and G. Wade, "Power and bandwidth efficient modulation and coding for small satellite communication terminals," in *Proc. IEEE ICC*, vol. 5, New York, Apr. 2002, pp. 2943–2946.

[4] A. Ambroze, M. Tomlinson, and G. Wade, "Magnitude modulation for small satellite earth terminals using QPSK and OQPSK," in *Proc. IEEE ICC*, vol. 3, Anchorage, Alaska, 2003, pp. 2099–2103.

[5] M. Gomes, F. Cercas, V. Silva, and M. Tomlinson, "Efficient M-QAM transmission using compacted magnitude modulation tables," in *Proc. IEEE GLOBECOM*, New Orleans, LA, Nov. 2008.

[6] M. Gomes, V. Silva, F. Cercas, and M. Tomlinson, "Low bback-off 16-APSK transmission using magnitude modulation and symbol quantization," in *Proc. IEEE IWSSC*, Toulouse, France, Oct. 2008, pp. 229–233.

[7] ——, "Power efficient back-off reduction through polyphase filtering magnitude modulation," *IEEE Commun. Lett.*, vol. 13, no. 8, pp. 606–608, Aug. 2009.

[8] ——, "Real-time lut-less magnitude modulation for peak power control of single carrier RRC filtered signals," in *Proc. IEEE SPAWC*, Perugia, Italy, June 2009, pp. 424–428.

[9] S. K. Mitra, *Digital Signal Processing: A Computer Based Approach. 3th ed.*, McGraw-Hill, 2006.

[10] "Digital video broadcasting (DVB); second generation framing structure, channel coding and modulation systems for broadcasting, interactive services, news gathering and other broadband satellite applications," ETSI Std. EN 302 307 V1.1.1, Mar. 2005.

[11] P. Rha and S. Hsu, "Peak-to-average ratio (PAR) reduction by pulse shaping using a new family of generalized raised cosine filters," in *Proc. IEEE VTC*, vol. 1, Oct. 2003, pp. 706–710.

[12] B. Chatelain and F. Gagnon, "Peak-to-average power ratio and intersymbol interference reduction by Nyquist pulse optimization," in *Proc. IEEE VTC*, vol. 2, Sept. 2004, pp. 954–958.

[13] M. Chen and O. Collins, "Trellis pruning for peak-to-average power ratio reduction," in *Proc. IEEE ISIT*, Sept. 2005, pp. 1261–1265.

[14] M. Tanahashi and H. Ochiai, "Near constant envelope trellis shaping for PSK signaling," *IEEE Trans. Commun.*, vol. 57, no. 2, pp. 450–458, Feb. 2009.

[15] M. Gomes, F. Cercas, V. Silva, and M. Tomlinson, "Polyphase magnitude modulation for peak power control," in *Proc. EUSIPCO*, Glasgow, Scotland, Aug. 2009.

[16] U. Mengali and A. N. D'Andrea, *Synchronization Techniques for Digital Receivers*. Plenum Press, 1997.

[17] H. Meyr, M. Moeneclaey, and S. Fechtel, *Digital Communication Receivers: Synchronization, Channel Estimation, and Signal Processing*. John Wiley & Sons, Inc., 1998.

[18] R. De Gaudenzi, A. Guillen, and A. Martinez, "Performance analysis of turbo-coded apsk modulations over nonlinear satellite channels," *IEEE Trans. Wireless Commun.*, vol. 5, no. 9, pp. 2396–2407, Sept. 2006.

[19] J. G. Proakis, *Digital Communications. 4th ed.*, McGraw-Hill, 2000.

[20] R. G. Gallager, "Low-density parity-check codes," *IRE Trans. Inform. Theory*, vol. IT-8, pp. 21–28, Jan. 1962.

[21] "Part 16: Air interface for fixed and mobile broadband wireless access systems—amendment for physical and medium access control layers for combined fixed and mobile operation in licensed nands," IEEE Std. 802.16e, 2005.

[22] J. Chen and M. Fossorier, "Near optimum universal belief propagation based decoding of low-density parity check codes," *IEEE Trans. Commun.*, vol. 50, no. 3, pp. 406–414, Mar. 2002.

[23] E. Sharon, S. Litsyn, and J. Goldberger, "An efficient message-passing schedule for ldpc decoding," in *Proc. IEEE Convention Electr. Electron. Engineers*, Sept. 2004, pp. 223–226.

[24] F. Harris, *Multirate Signal Processing for Communication Systems*. Prentice Hall PTR, 2004.

[25] M. Gomes, V. Silva, F. Cercas, and M. Tomlinson, "Analytical analysis of polyphase magnitude modulation method's performance," in *Proc. IEEE ICC*, Cape Town, South Africa, May 2010.

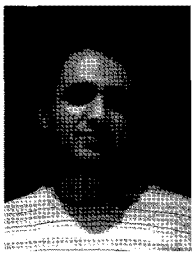

Marco Gomes received his graduation Diploma and M.Sc. in Electrical and Computer Engineering from the University of Coimbra, Portugal, in 2000 and 2004, respectively. He's currently a Ph.D. Student and also a Teaching Assistant at the Department of Electrical and Computer Engineering, University of Coimbra, where he lectures signal processing, electronics and electric circuits. His research activities are mainly carried out at the Instituto de Telecomunicações, Coimbra, Portugal. His main research interests focus on signal processing, satellite communications, channel coding, and ultra wide band communications.

Francisco Cercas received his Licenciatura, M.Sc., and Ph.D. degrees from Instituto Superior Técnico (IST), Technical University of Lisbon, Portugal, in 1983, 1989, and 1996, respectively. He worked for the Portuguese Industry as a research engineer and developed the work of his M.S. and Ph.D. theses as an Invited Researcher at the Satellite Centre of the University of Plymouth, U.K. This resulted in new contributions for the characterization of direct digital frequency synthesizer (DDS) signals and in a new class of codes named TCH after Tomlinson, Cercas and Hughes. He lectured during 15 years at IST and became Associate Professor in 1999 at ISCTE-Lisbon University Institute, Lisbon, where he is the Head of the School of Technology and Architecture. He has over 100 international publications with referees including conferences, magazines, book chapters and a patent. His main research interests focus on mobile and personal communications, satellite communications, channel coding, and ultra wide band communications.

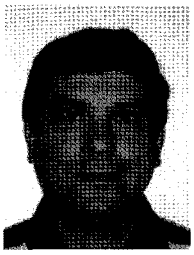

Vitor Silva received the graduation Diploma and Ph.D. degrees in Electrical Engineering from the University of Coimbra, Portugal, in 1984 and 1996, respectively. He is currently an Auxiliary Professor in the Department of Electrical and Computer Engineering, University of Coimbra, where he lectures signal processing and information and coding theory. His research activities in signal processing, image and video compression, coding theory, and parallel computing are mainly carried out at the Instituto de Telecomunicações, Coimbra, Portugal. He published more than 110 papers in journals and international conferences.

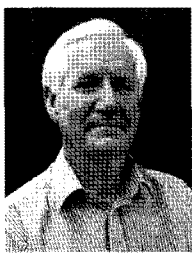

Martin Tomlinson is best known for the invention of the Tomlinson-Harashima precoding technique. He received his Ph.D. from Loughborough University in 1970 on the subject of adaptive equalization for data transmission and worked at Plessey Telecommunications Research Ltd until 1975 in digital communication and satellite transmission. He then spent seven years in the Satellite Communications Division of RSRE (now Qinetiq) where he worked on the Skynet space and ground segments. He was also Project Manager for the communications sub-system of the NATO IV satellite before joining the University of Plymouth as the Head of the Communication Engineering Department in 1982. He is an Emeritus Professor leading research projects in communications, coding, signal processing, encryption, and watermarking. He has published over 200 papers in the fields of digital modulation and coding, signal processing, video coding, and satellite communications, as well as contributing to various standards such as the DVB-RCS standard for small terminals. He has filed over 50 patents and is a Member of the IET, a Senior Member of the IEEE, Member of the Information Theory Society, Communications Society (ComSoc), and a Member of the IEEE Satellite and Space Communications Society.